

RESEARCH

Open Access



# Quantification and Modeling of the Interactions of Gamma Radiation with Concrete from Bulk-Scale Observations

Yonathan Reches\*

## Abstract

The exposure of concrete to gamma radiation gives rise to a set of physical and chemical processes over multiple length scales, from molecular to bulk. The literature includes a number of bulk-scale studies which report the radiogenic heating of concrete and the loss of water (unbound, physically-bound, and/or chemically-bound) due to irradiation. This paper mechanistically quantifies observations by these studies, and presents a continuum framework to model the effects of gamma photons on concrete. A basis is presented for comparing otherwise disparate results in the literature for radiolysis rates. The Stefan–Boltzmann Law, adapted to include a gamma heat source term, reasonably describes radiogenic heating in concrete specimens. In multiple studies, the primary mechanism for dehydration is the loss of liquid water in the pore network of the cement product, rather than of water which is physically or chemically bound in a solid state.

**Keywords:** cement, concrete, mortar, radiation, modeling, radiogenic heating, radiolysis, dehydration

## 1 Introduction

This is a companion paper to Reches 2019 (Under review), which summarizes experimental observations of the multi-scale effects of gamma rays on concrete. The present paper details quantitative and modeling approaches used to describe these effects.

Gamma radiation affects concrete on multiple length-scales, from the molecular- to the bulk-scale. The literature includes a number of bulk-scale observations related to the radiogenic heating of concrete (Linton et al. 2018; Sanchez et al. 2018) and the radiolysis of water (unbound, physically-bound, and/or chemically-bound) (Gray 1972; Kelly et al. 1969; Kontani et al. 2010; 2013). The present work uses data from these studies as a basis to construct mechanistic models, which may support the design of future experiments and systems related to the application of concrete in conditions of gamma radiation (e.g., dry cask nuclear storage). A basis is presented for comparing

otherwise disparate results in the literature for radiolysis rates. The comparative basis for other properties of interest, such as strength and porosity, is shown in Appendix A.

## 2 Modeling of Radiogenic Heating

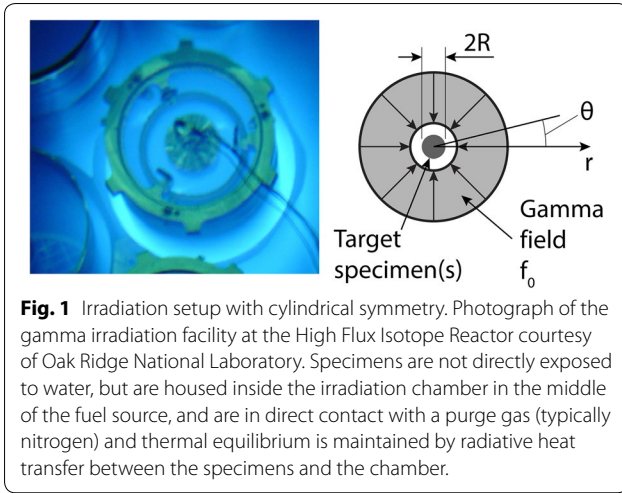
This section supports modeling of radiogenic heating in specimens of cement products, corresponding with Sub-Sect. 5.2 of the companion paper.

### 2.1 Model for Radiogenic Heating of Irradiated Target in Cylindrically-Symmetric Gamma Irradiation Configuration

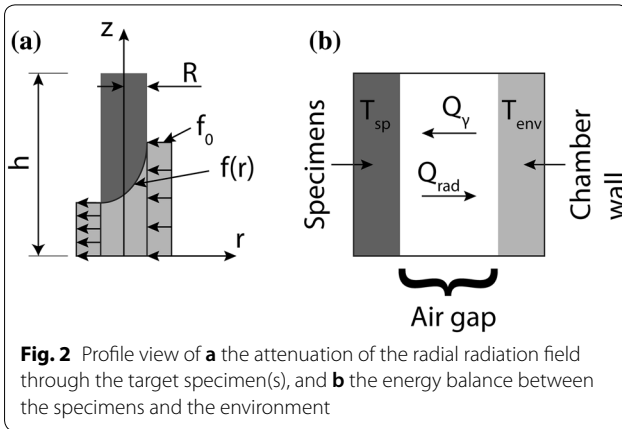
It is common for the radiation field in studies involving the gamma irradiation of cement products to have a cylindrical symmetry, and for the specimens to have a cylindrical (or quasi-cylindrical) geometry. Such a configuration is shown in Fig. 1 for the conditions reported in Linton et al. (2018) and Sanchez et al. (2018).

Figure 2 shows the attenuation of the gamma radiation field as it passes through the target specimens. Per

\*Correspondence: yonathanreches@gmail.com  
US Air Force Space and Missile Systems Center, Los Angeles Air Force Base, 483 N Aviation Blvd, El Segundo, CA 90245, USA  
Journal information: ISSN 1976-0485 / eISSN 2234-1315



**Fig. 1** Irradiation setup with cylindrical symmetry. Photograph of the gamma irradiation facility at the High Flux Isotope Reactor courtesy of Oak Ridge National Laboratory. Specimens are not directly exposed to water, but are housed inside the irradiation chamber in the middle of the fuel source, and are in direct contact with a purge gas (typically nitrogen) and thermal equilibrium is maintained by radiative heat transfer between the specimens and the chamber.



**Fig. 2** Profile view of **a** the attenuation of the radial radiation field through the target specimen(s), and **b** the energy balance between the specimens and the environment

William et al. (2013), the attenuation follows an exponential law (1).

$$f(r) = f_0 \exp[-\mu(R - r)] \tag{1}$$

where  $f_0$  is the incident gamma radiation dose rate at the exterior surface of the specimens ( $\text{W/kg} = 3.6 \text{ kGy/h}$ ),  $\mu$  is the linear attenuation coefficient of the material for gamma rays ( $\text{m}^{-1}$ ),  $R$  is the radius of the set of specimens (m), and  $r$  is the radial dimension after Fig. 1 (m).

As the gamma beam travels through the specimen and is attenuated according to (2), the photonic energy is converted to thermal energy  $Q_\gamma$ , given by (3) and (4).

$$\frac{df}{dr} = f_0 \exp[-\mu(R - r)] \tag{2}$$

$$Q_\gamma = \int_0^h \int_0^{2\pi} \int_{-R}^R \left( \frac{df}{dr} r \right) \rho dr d\theta dz$$

$$= 2\pi h \rho f_0 \left\{ -\frac{\mu r + 1}{\mu^2} \exp[\mu(R - r)] \right\} \Big|_{r=-R}^R \tag{3}$$

$$Q_\gamma = 2\pi h \rho f_0 \frac{1}{\mu^2} [(\mu R - 1) \exp(2\mu R) + \mu R + 1] \tag{4}$$

where,  $\theta$  is the angular dimension after Fig. 1 (m),  $z$  is the height dimension after Fig. 2 (m),  $h$  is the height of specimen(s) after Fig. 2 (m), and  $\rho$  is the density of specimen(s) ( $\text{kg/m}^3$ ).

Due to the sufficiently high thermal conductivity of concrete, let us estimate that the temperature does not substantially vary within a specimen, per Sanchez et al. (2018). The radiative energy balance between the specimen and its environment is given by the Stefan–Boltzmann Law (5) (Boltzmann 1884).

$$Q_{rad} = \varepsilon \sigma A (T_{sp}^4 - T_{env}^4) \tag{5}$$

where  $Q_{rad}$  is the radiative heat flux from the specimen to its environment (W),  $\varepsilon$  is the emissivity of the apparatus,  $\sigma$  is the Stefan–Boltzmann constant ( $5.67 \times 10^{-8} \text{ Wm}^{-2} \text{ K}^{-4}$ ),  $A$  is the exposed area of specimen ( $\text{m}^2$ ),  $T_{sp}$  is the temperature of the specimen (K), and  $T_{env}$  is the temperature of the environment (K).

The emissivity of the apparatus is given by (6).

$$\varepsilon = \frac{1}{\frac{1}{\varepsilon_1} + \frac{1}{\varepsilon_2} - 1} \tag{6}$$

where  $\varepsilon_1$  is the emissivity of the concrete or encasing material (such as a canister or foil wrapping), and  $\varepsilon_2$  is the emissivity of the irradiation chamber wall.

In steady-state conditions, assuming cylindrical geometry, the energy balance yields (7)–(9).

$$Q_\gamma = Q_{rad} \tag{7}$$

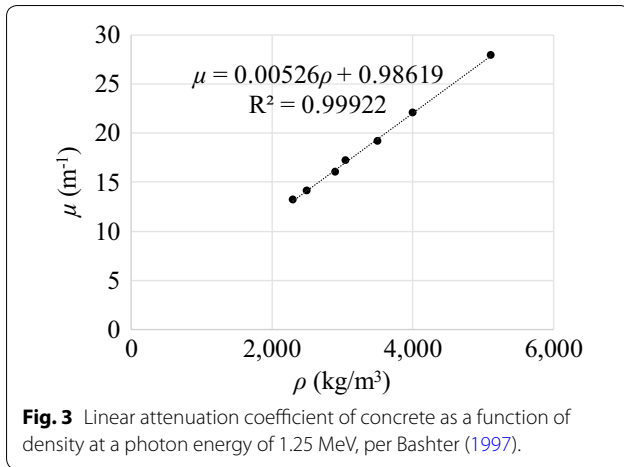
$$Q_\gamma = 2\pi R h \varepsilon \sigma (T_{sp}^4 - T_{env}^4) \tag{8}$$

$$T_{sp} = \left( \frac{Q_\gamma}{2\pi R h \varepsilon \sigma} + T_{env}^4 \right)^{1/4} \tag{9}$$

### 2.2 Estimating the Linear Attenuation Coefficient

Bashter (1997) tabulated the linear attenuation coefficient  $\mu$  of concrete by energy of the incident photons and density of the concrete  $\rho$ .  $^{60}\text{Co}$  has two major gamma peaks at 1.17 and 1.33 MeV, so the linear attenuation coefficients reported by Bashter at 1.25 MeV were used. The relationship of  $\mu$  vs.  $\rho$  for the seven mixes examined therein was linear, per Fig. 3, with the linear regression (10).

$$\mu = 0.00526\rho + 0.98619 \tag{10}$$



**2.3 Application of the Model to Sanchez et al. (2018)**

The model (9), is validated using Sanchez et al. (2018). The authors reported specimen geometry as  $2.54 \times 2.54 \times 5.08 \text{ cm}^3$  (1"  $\times$  1"  $\times$  2") prisms, which were arranged in 11 layers, each containing 4 specimens in a square pattern, shown in Fig. 4. Though not perfectly cylindrical, this geometry, when modeled as quasi-cylindrical, yields  $R = 2.54 \times 10^{-2} \text{ m}$ . The specimens were irradiated at the High Flux Isotope Reactor, where  $T_{env} = 310.93 \text{ K}$  (100 °F) (Oak Ridge National Laboratory). The density of the specimens was  $\rho = 3200 \text{ kg/m}^3$ , yielding  $\mu = 17.8 \text{ m}^{-1}$  per (10).

Specimens were encased in a stainless steel canister (Fig. 4), which was perforated so that 70% of its profile was unpolished steel (emissivity of 0.7 (Emissivity

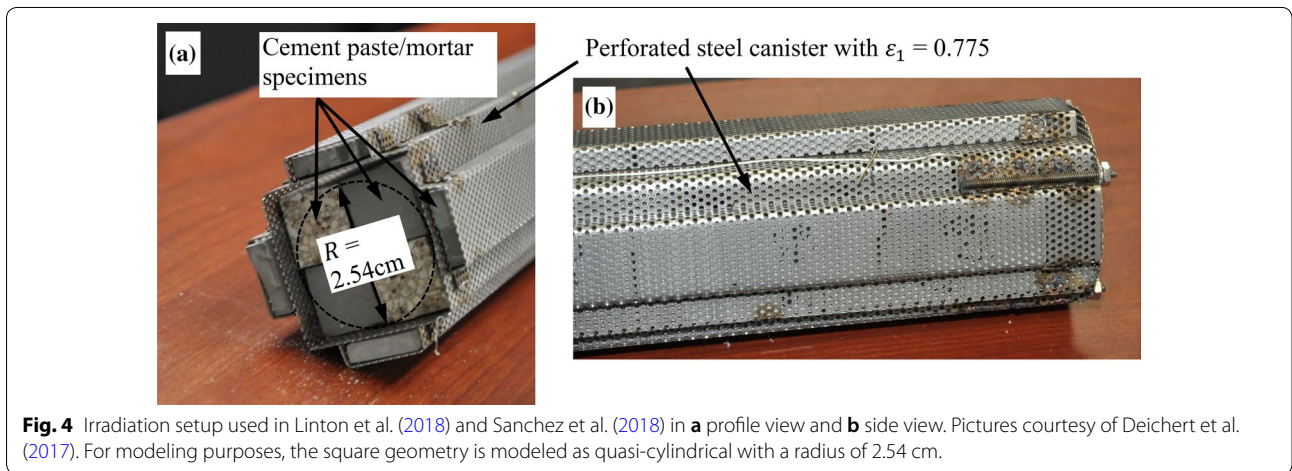


**Table 1** Observed and modeled  $T_{sp}$  with associated sum of square of errors, sum of squares, and r-squared.

$f_0$		$Q_y$ (W)	$T_{sp}$ (K)		Square of error	Square
( $10^4$ Gy/h)	(W/kg)		Modeled	Measured		
1.9	5.4	1.7	355	349	32	11,524
4.7	13.1	4.2	397	374	551	6798
6.6	18.4	5.9	421	397	566	3534
13.6	37.7	12.0	483	442	1666	203
25.2	70.0	22.3	552	528	556	5206
37.0	102.8	32.8	603	648	2010	36,615
Average				456		
Sum					5380	63,880
r-squared						0.92

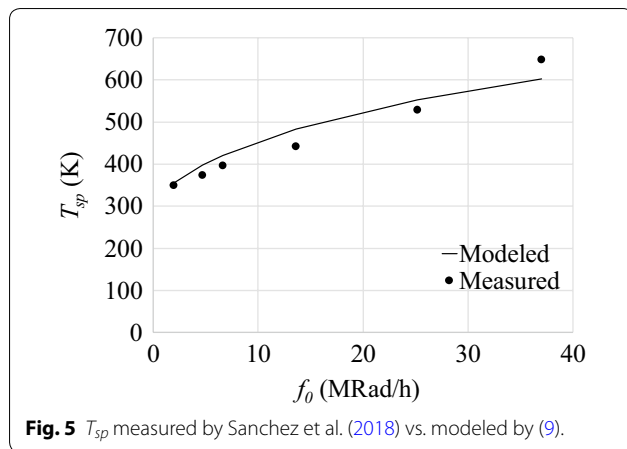


Fig. 5  $T_{sp}$  measured by Sanchez et al. (2018) vs. modeled by (9).

in the Infrared 2018) and 30% was exposed concrete (emissivity 0.95) (Emissivity in the Infrared 2018). By the weighted average,  $\varepsilon_1=0.775$ . The irradiation chamber wall consisted of unpolished stainless steel ( $\varepsilon_2=0.7$ ) (Emissivity in the Infrared 2018). Therefore, per (6),  $\varepsilon=0.582$ .

Per Table 1 and Fig. 5, this model reasonably describes the radiogenic heating of the specimens. Considering that this approach does not require any fitting parameters, the r-squared value of 0.92 is satisfactory.

### 3 Rates of Radiolysis

This section supports modeling of the fate of water in gamma-irradiated cement products, corresponding with Sub-Sect. 5.3 of the companion paper.

For cement products subjected to gamma radiation, unbound water may be lost due to a combination of radiation-related effects (dehydration or radiolysis by direct impact of photons) and non-radiation related effects (evaporation due to temperature and humidity conditions). For temperatures near or below 100 °C, physically- or chemically-bound water is essentially only lost due to the radiation-related effects. A first-order model for gamma-related dehydration of water in cementitious matrices is developed below based on data from Gray (1972), Kelly et al. (1969), Kontani et al. (2010, 2013). Given the innate challenge of applying a new model to data which were not designed for such an analysis, a number of simplifying assumptions were required. In all cases, dehydration was assumed to be independent of specimen geometry (essentially, it was assumed that the rate of formation of radiolytic products was slower than the rate of their outward diffusion, which seems likely, given the small specimen sized used in all these studies) and the directionality of the gamma radiation field.

The approach in these cases was to report the water (Kontani et al. 2010), H<sub>2</sub> gas (Kontani et al. 2010, 2013),

and/or total gas volume (Gray 1972; Kelly et al. 1969) that evolved from the specimens, as well as the initial (Gray 1972; Kelly et al. 1969; Kontani et al. 2010, 2013) and/or final (Kontani et al. 2010, 2013) water content of the specimens. Regardless of the reaction pathways, if we assume that the net stoichiometry of water radiolysis is approximately per (11), then these data can be used to construct the mass balance (12) for radiolysis and dehydration.



$$\frac{d}{dt} (m_{w,s} + m_{w,l} + m_{w,g} + m_{w,e} + m_{H_2,e} + m_{O_2,e}) = 0 \tag{12}$$

where  $t$  is the time (h),  $m_{w,s}$ ,  $m_{w,l}$ ,  $m_{w,g}$  is the mass of solid (i.e., chemically-bound and some physically-bound), liquid (i.e., unbound and some physically-bound), and gaseous water, respectively, in the specimen or element (g), and  $m_{w,e}$ ,  $m_{H_2,e}$ ,  $m_{O_2,e}$  is the mass of water vapor, H<sub>2</sub>, and O<sub>2</sub>, respectively, evolved from the specimen or element to the atmosphere from an arbitrarily selected start time  $t_0$  to  $t$  (g).

At present, there does not appear to be some fundamental criterion to determine the degree to which physically-bound water can be classified as  $m_{w,s}$  vs.  $m_{w,l}$ . Such a distinction would make an interesting topic for future research, but is not strictly necessary for the analysis in this paper. Supposing that the mass of gaseous water in the specimen or element is fairly constant and applying the stoichiometry from (11), the mass balance is simplified to (13). Then (14) and (15) describe the net hydrolysis rates.

$$\frac{d}{dt} (m_{w,s} + m_{w,l} + m_{w,e} + 9m_{H_2,e}) = 0 \tag{13}$$

$$m_{w,s} \rightarrow 9m_{H_2,e} \quad K_{r,s} \tag{14}$$

$$m_{w,l} \rightarrow 9m_{H_2,e} \quad K_{r,l} \tag{15}$$

where  $K_{r,s}$  is the net rate of radiolysis of solid-state water (Gy<sup>-1</sup>), and  $K_{r,l}$  is the net rate of radiolysis of liquid water (Gy<sup>-1</sup>). The general solution (13) lends itself to a multitude of test configurations and boundary conditions. Particular solutions for the conditions described in Gray (1972), Kelly et al. (1969), Kontani et al. (2010, 2013) are presented below.

#### 3.1 Kontani et al. (2013)

In Kontani et al. (2013), a first set of specimens was fired at 120 °C, then irradiated at 25–60 °C. For these specimens, the authors reported that  $m_{w,l}, m_{w,e} \approx 0$ .

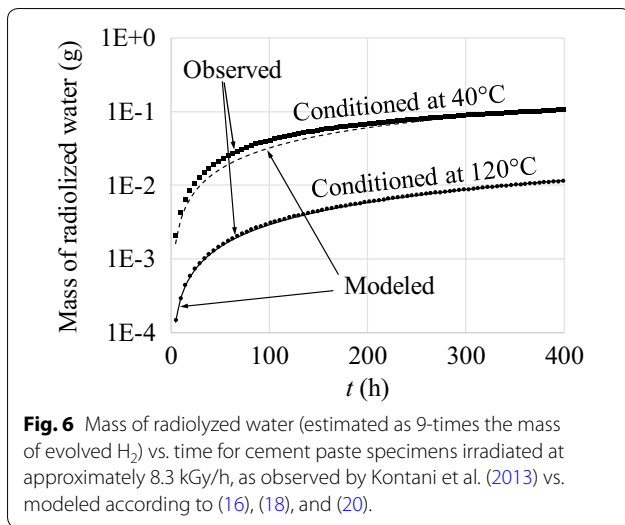


**Fig. 6** Mass of radiolyzed water (estimated as 9-times the mass of evolved H<sub>2</sub>) vs. time for cement paste specimens irradiated at approximately 8.3 kGy/h, as observed by Kontani et al. (2013) vs. modeled according to (16), (18), and (20).

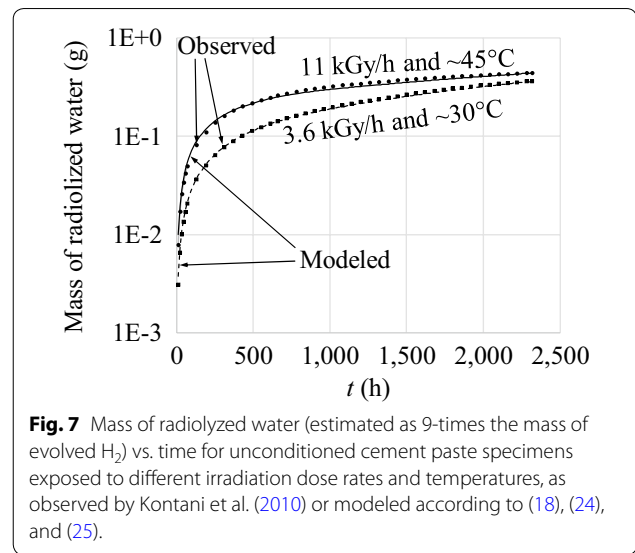


**Fig. 7** Mass of radiolyzed water (estimated as 9-times the mass of evolved H<sub>2</sub>) vs. time for unconditioned cement paste specimens exposed to different irradiation dose rates and temperatures, as observed by Kontani et al. (2010) or modeled according to (18), (24), and (25).

Assuming, therefore, that  $\frac{dm_{w,l}}{dt}, \frac{dm_{w,e}}{dt} = 0$ ,  $K_{r,s}$  is then given by (16).  $\frac{dm_{H_2,e}}{dt}, m_{w,s}, f_0$ , and  $t_f$  were reported.

$$K_{r,s} = \frac{\int_0^{t_f} 9 \frac{dm_{H_2,e}}{dt} dt}{m_{w,s} f_0 t_f} \tag{16}$$

where  $t_f$  is the time of termination of experiment (h).

A second set of specimens was fired at 40 °C, then irradiated at 25–60 °C. For these specimens, the authors reported that  $\frac{dm_{H_2,e}}{dt} \ll \frac{dm_{w,e}}{dt}, \frac{dm_{w,s}}{dt} \ll \frac{dm_{w,l}}{dt}$ , and the total water content in the specimens decreased linearly with time. The latter two observations imply  $\frac{d}{dt}(m_{w,s} + m_{w,l}) \approx \frac{dm_{w,l}}{dt} \approx C$ , where  $C$  is a constant. Together, these approximations give rise to (17) and (18). The integration of (18) from the experimental start time  $t = 0$  to the experimental end time  $t = t_f$  yields (19). Given that the vast majority of solid water is stable at 120 °C (Lee et al. 2009), it is assumed that  $K_{r,s}$  for any specimen fired to 40 °C was the same as the same specimen’s counterparts which had been fired to 120 °C. Then  $K_{r,l}$  is given by (20). This model reasonably described observations of the net hydrolysis of water (e.g., Fig. 6).

$$m_{w,l}(t) = m_{w,l,i} - \frac{t}{t_f}(m_{w,l,i} - m_{w,l,f}) \tag{17}$$

$$9 \frac{dm_{H_2,e}}{dt} = (K_{r,l} m_{w,l} + K_{r,s} m_{w,s}) f_0 \tag{18}$$

$$9 m_{H_2,e,f} = \left[ K_{r,l} \cdot \frac{1}{2} (m_{w,l,i} + m_{w,l,f}) + K_{r,s} m_{w,s} \right] f_0 t_f \tag{19}$$

$$K_{r,l} = \frac{\frac{9 m_{H_2,e,f}}{f_0 t_f} - K_{r,s} m_{w,s}}{\frac{1}{2} (m_{w,l,i} + m_{w,l,f})} \tag{20}$$

where  $m_{w,l,i}, m_{w,l,f}$  is the mass of liquid water measured in the specimen in the initial and final condition, respectively (g).

### 3.2 Kontani et al. (2010)

In Kontani et al. (2010), two sets of specimens were irradiated: (i) at 11 kGy/h and approximately 45 °C (4 replicates) and (ii) at 3.6 kGy/h and approximately 30 °C (2 replicates). In this study, the total water content  $m_{w,t} = m_{w,s} + m_{w,l}$  was reported at  $t = 0$ .  $\frac{dm_{H_2,e}}{dt}$  and  $\int_0^t \frac{dm_{w,l}}{dt} dt$  were reported for all  $0 \leq t \leq t_f$ . The experiment was run until essentially all liquid water had evaporated (i.e.,  $m_{w,l} \approx 0$  at  $t = t_f$ ). Accordingly,  $K_{r,l}$  and  $K_{r,s}$  were estimated by a least sum of square of errors regression of (21), with  $m_{w,s}$  and  $m_{w,l}$  determined according to (22) and (23), respectively. This model reasonably described observations of the net hydrolysis of water (e.g., Fig. 7).

$$9 \frac{dm_{H_2,e}}{dt} = (K_{r,l} m_{w,l} + K_{r,s} m_{w,s}) f_0 \tag{21}$$

$$m_{w,s} = m_{w,t}(t = 0) - m_{w,l}(t = 0) = m_{w,t} - \int_0^{t_f} \frac{dm_{w,l}}{dt} dt \tag{22}$$

$$m_{w,l}(t) = m_{w,t} - m_{w,s} - \int_0^t \frac{dm_{w,l}}{dt} dt \tag{23}$$

**3.3 Kelly et al. (1969) and Gray (1972)**

A set of identical data were presented by Kelly et al. (1969) and by Gray (1972) for gamma irradiation of concrete specimens at 50 kGy/h circa room temperature. The flux of gases evolved from the specimens was reported and consisted essentially of O<sub>2</sub> and H<sub>2</sub>, with minor amounts of N<sub>2</sub> and CO. The authors estimated that the water content at the start of irradiation was  $m_{w,t}(t = 0) = 0.05$  kg/kg concrete, but did not specify how much was solid vs. liquid. If we assume that the solid-state water was approximately 14% of the mass of cement [per Kontani et al. (2013)] and the remainder was liquid, then  $m_{w,s} = 0.034$  kg/kg concrete, and  $m_{w,l} = 0.016$  kg/kg concrete.

Kelly et al. (1969) and Gray (1972) reported for radiation doses  $\leq 2.27 \times 10^7$  Gy a gas flux that averaged 23 cm<sup>3</sup>/MGy/kg concrete at standard temperature and pressure. The specimens were then removed from the irradiation rig for 1 month. During that time, the specimens appear to have (perhaps inadvertently) been desiccated of all liquid water, so that for doses  $> 2.27 \times 10^7$  Gy the gas flux decreased to 2.4 cm<sup>3</sup>/MGy/kg concrete at standard temperature and pressure.

In order to use this reported volumetric flux in the present models, it is necessary to convert to a mass flux term, using the idealized gas assumption at standard

temperature and pressure (1 mol =  $2.24 \times 10^4$  cm<sup>3</sup>). Thus, the molar fluxes are  $1.02 \times 10^{-3}$  mol/MGy/kg concrete (for doses  $\leq 2.27 \times 10^7$  Gy) and  $1.06 \times 10^{-4}$  mol/MGy/kg concrete (for doses  $> 2.27 \times 10^7$  Gy). Assuming that the evolved gas consisted of H<sub>2</sub> and O<sub>2</sub> according to the stoichiometry of (11), then the mass fluxes  $\frac{d}{d(f_0t)}(m_{H_2,e} + m_{O_2,e})$  are  $6.11 \times 10^{-3}$  g H<sub>2</sub>O/MGy/kg concrete (for doses  $\leq 2.27 \times 10^7$  Gy) and  $6.37 \times 10^{-4}$  g H<sub>2</sub>O/MGy/kg of concrete (for doses  $> 2.27 \times 10^7$  Gy). Then  $K_{r,l} = 3.8 \times 10^{-10}$  Gy<sup>-1</sup> per (24) and  $K_{r,s} = 1.9 \times 10^{-11}$  Gy<sup>-1</sup> per (25).

$$K_{r,l} = \left[ \frac{d}{d(f_0t)}(m_{H_2,e} + m_{O_2,e}) - K_{r,s}m_{w,s} \right] / m_{w,l}$$

for doses  $\leq 2.27 \times 10^7$  Gy (24)

$$K_{r,s} = \frac{\frac{d}{d(f_0t)}(m_{H_2,e} + m_{O_2,e})}{m_{w,s}}$$

for doses  $> 2.27 \times 10^7$  Gy (25)

**3.4 Results**

The values of  $K_{r,s}$  and  $K_{r,l}$  calculated using data from Gray (1972), Kelly et al. (1969), Kontani et al. (2010, 2013) and the associated conditions are summarized in Table 2. For all

**Table 2 Experimental matrices with associated values of  $K_{r,s}$  and  $K_{r,l}$ .**

Conditioning temperature (°C)	Exposure temperature (°C)	$f_0$ (10 <sup>2</sup> Gy/h)	Replicates	$K_{r,s}$ (10 <sup>-10</sup> Gy <sup>-1</sup> )	$K_{r,l}$ (10 <sup>-10</sup> Gy <sup>-1</sup> )
<b>Kontani et al. (2013)</b>					
120	60	83.9	2	Per (16)	Per (20)
120	60	42.8	2	0.82, 0.82	
120	60	9.2	2	0.64, 0.86	
120	60	9.2	2	0.67, 0.69	
120	40	42.8	2	0.79, 0.86	
120	40	9.2	2	0.49, 0.52	
120	25	9.2	2	0.20, 0.36	
40	60	82.3	2	0.82, 0.82 <sup>a</sup>	11, 12
40	60	42.7	2	0.75, 0.75 <sup>a</sup>	13, 13
40	60	9.3	2	0.68, 0.68 <sup>a</sup>	18, 17
40	40	42.7	2	0.82, 0.82 <sup>a</sup>	12, 13
40	40	9.3	2	0.51, 0.51 <sup>a</sup>	13, 13
40	25	9.3	2	0.28, 0.28 <sup>a</sup>	12, 11
Mean ± standard deviation				0.64 ± 0.21	13 ± 2
<b>Kontani et al. (2010)</b>					
N/A	~45	110	4	Per (21)	Per (21)
N/A	~30	36	2	3.8, 2.3, 1.6, 1.5	13, 18, 20, 21
Mean ± standard deviation				1.7, 0.59	5.0, 7.4
Mean ± standard deviation				1.9 ± 1.1	14 ± 7
<b>Kelly et al. (1969) and Gray (1972)</b>					
N/A	20	500	1	Per (25)	Per (24)
				0.19	3.8

<sup>a</sup> From equivalent set conditioned at 120 °C.

studies,  $K_{r,s}$  was on the order of  $10^{-11}$ – $10^{-10}$  Gy<sup>-1</sup> and  $K_{r,l}$  was on the order of  $10^{-10}$ – $10^{-9}$  Gy<sup>-1</sup>. For any given material and configuration, it was observed that  $K_{r,s} \ll K_{r,l}$ . Therefore, it is understood that the primary pathway for radiolysis of water occurs through the liquid water. The data currently available in the literature are not sufficient to determine the effects of composition, specimen geometry, and environmental conditions on  $K_{r,s}$  and  $K_{r,l}$ .

#### 4 Conclusions

The gamma radiogenic heating of concrete was successfully modeled using the Stefan–Boltzmann Law by incorporating a term to account for thermal energy flux due to gamma radiation.

A general solution was developed for mass balances related to the radiolysis of water and cement products and outward diffusion of the generated H<sub>2</sub> and O<sub>2</sub> gases. Previous studies (Gray 1972; Kelly et al. 1969; Kontani et al. 2010, 2013), have reported mass/volume observations for water and/or radiolytic products evolved during gamma irradiation of cement products in a variety of conditions. These observations were used to develop particular solutions, which showed that radiolysis occurs primarily in the liquid (i.e., unbound and some physically-bound) water and secondarily in the solid (i.e., chemically-bound and some physically-bound) water.

In order to support a further validation and development of this model, future irradiation work on concrete may include the following experimental facets: (i) characterization of effluent gases from the irradiation chamber (e.g., by gas chromatography-mass spectrometry) in order to determine the mass balance of radiolyzed vs. non-radiolyzed off-gases, (ii) irradiation of specimens of varying geometry in comparable conditions, in order to determine the effects of diffusion pathways on the mass balances of water and radiolytic products, and (iii) additional work providing temperature control and monitoring, similar to Kontani et al. 2013, in order to allow for de-coupling of temperature and radiation effects.

#### Acknowledgements

The support of Dr. Timothy Ault, Prof. Florence Sanchez, and Prof. David S. Kosson is gratefully acknowledged. This work did not receive any specific grant from funding agencies in the public, commercial, or not-for-profit sectors. The views expressed in this article do not necessarily represent the views of the Air Force or the United States.

#### Authors' contributions

The author read and approved the final manuscript.

#### Funding

Not applicable.

#### Availability of data and materials

The data used in this paper are available in the published sources (Bashter 1997; Deichert et al. 2017; Gray 1972; Kelly et al. 1969; Kontani et al. 2010, 2013; Linton et al. 2018; Reches Under review; Sanchez et al. 2018).

#### Competing interests

The author declares no competing interests.

## Appendix A

### Variability in Strength and Porosity Data

This section details the estimation of variability of data found in the literature for compressive strength, tensile strength, and porosity of irradiated vs. non-irradiated specimens. The data are summarized in Sub-Sects. 5.5 and 5.6 of the companion paper (Reches Under review).

The various studies on this subject were carried out with different materials, ages, specimen geometries, etc. Therefore, even in the control specimens (i.e., in a non-irradiated condition), properties of interest  $p_c$  (e.g., compressive strength) varied from study to study. However, in comparing multiple studies, the interest is not in the property of the control specimens, but in how gamma radiation affected the property, which we will capture in the distribution  $p_\Delta$ , which is normalized to  $p_c$ . Let us suppose that  $p_c$  follows a normal distribution (26) and that the same property of the target (i.e., irradiated) specimens  $p_t$  for a given radiation dose follows a normal distribution (27). Then  $p_\Delta$  will also follow a normal distribution, given by (28).

$$p_c \sim N(\bar{x}_c, s_c^2) \tag{26}$$

$$p_t \sim N(\bar{x}_t, s_t^2) \tag{27}$$

$$p_\Delta \sim N\left(\frac{\bar{x}_t}{\bar{x}_c}, \frac{s_t^2 + s_c^2}{\bar{x}_c^2}\right) \tag{28}$$

where  $p_c$ ,  $p_t$  is the property of interest such as compressive/tensile strength (MPa) or porosity (%) for control and target (i.e., irradiated) specimens, respectively,  $p_\Delta$  is the comparative basis for how gamma radiation affects the property between control and target specimens,  $\bar{x}_c$ ,  $\bar{x}_t$  is the mean of measurements of property for control and target specimens, respectively,  $s_c^2$ ,  $s_t^2$  is the observed variability of property for control and target specimens, respectively.

For data from Maruyama et al. (2018), Sommers (1969), Soo and Milian (1989, 2001), all of the parameters used herein were reported, so that the standard deviation (the uncertainty bounds) of the property of interest relative to the control was given by  $\frac{\sqrt{s_t^2 + s_c^2}}{\bar{x}_c}$ . For data from Gray (1972), Kelly et al. (1969), Sopko et al. (2004), Vodák et al. (2005),  $s_t^2$  was reported (apparently pooled) and  $s_c^2$  was not reported. However, it appears that  $s_c^2 \ll s_t^2$ , so that

the standard deviation of the property of interest relative to the control would approximately be given by  $\frac{\sqrt{s_L^2}}{\bar{x}_c}$ . For the single datum from Alexander (1963), no variability metric was reported for the target or control cases.

Received: 6 July 2019 Accepted: 9 September 2019  
Published online: 09 December 2019

## References

- Alexander, S. (1963). In Hilsdorf 1978. *Effects of Irradiation on Concrete Final Results. Technical Report HL.63/6438*. Retrieved from <http://large.stanford.edu/courses/2015/ph241/anzelmo1/docs/hilsdorf.pdf>.
- Bashter, I. (1997). Calculation of radiation attenuation coefficients for shielding concretes. *Annals of Nuclear Energy*, 24(17), 1389–1401.
- Boltzmann, L. (1884). Ableitung des Stefan'schen Gesetzes, betreffend die Abhängigkeit der Wärmestrahlung von der Temperatur aus der electromagnetischen Lichttheorie. *Annalen der Physik*, 258(6), 291–294.
- Deichert, G. G., Linton, K. D., Terrani, K. A., Selby, A. P., & Reches, Y. (2017). *Vanderbilt University Gamma Irradiation of Nano-modified Concrete (2017 Milestone Report)*. Retrieved from <https://info.ornl.gov/sites/publications/Files/Pub101533.pdf>.
- Emissivity in the Infrared. (2018). Retrieved from <https://www.optotherm.com/emiss-table.htm>.
- Gray, B. (1972). *Effects of reactor radiation on cements and concrete*. In: Paper presented at the results of concrete irradiation programmes, Brussels, Belgium.
- Kelly, B., Brocklehurst, J., Mottershead, D., McNearney, S., & Davidson, I. (1969). *The effects of reactor radiation on concrete*. In: Paper presented at the 2nd conference on prestressed concrete pressure vessels and their insulation, London, 1969.
- Kontani, O., Ichikawa, Y., Ishizawa, A., Takizawa, M., & Sato, O. (2010). Irradiation effects on concrete structures. *International symposium on the ageing management and maintenance of nuclear power plants*, pp. 173–182.
- Kontani, O., Sawada, S., Maruyama, I., Takizawa, M., & Sato, O. (2013). *Evaluation of irradiation effects on concrete structure: Gamma-ray irradiation tests on cement paste*. In: Paper presented at the ASME 2013 power conference.
- Laboratory, O. R. N. *Gamma irradiation facility at HFIR*. Retrieved from <https://neutrons.ornl.gov/hfir/gamma-irradiation>.
- Lee, J., Xi, Y., Willam, K., & Jung, Y. (2009). A multiscale model for modulus of elasticity of concrete at high temperatures. *Cement and Concrete Research*, 39(9), 754–762.
- Linton, K., Reches, Y., Teising, R., Sanchez, F., & Kosson, D. (2018). *Low and High Temperature Gamma Irradiations of Nano-Modified Concrete in the High Flux Isotope Reactor*. Retrieved from <https://info.ornl.gov/sites/publications/Files/Pub101533.pdf>.
- Maruyama, I., Ishikawa, S., Yasukouchi, J., Sawada, S., Kurihara, R., Takizawa, M., et al. (2018). Impact of gamma-ray irradiation on hardened white Portland cement pastes exposed to atmosphere. *Cement and Concrete Research*, 108, 59–71.
- Reches, Y. (Under review). The multi-scale effects of gamma radiation on concrete. *Results in Materials*.
- Sanchez, F., Kosson, D., Brown, K., Delapp, R., Teising, R., Gonzalez, R.,... Helbing, M. (2018). *Development of nano-modified concrete for next generation of storage systems*. Retrieved from <https://www.osti.gov/servlets/purl/1469196>.
- Sommers, J. F. (1969). Gamma radiation damage of structural concrete immersed in water. *Health Physics*, 16(4), 503–508.
- Soo, P., & Millian, L. (1989). *Sulfate-attack resistance and gamma-irradiation resistance of some portland cement based mortars*. Retrieved from <https://www.nrc.gov/docs/ML1322/ML1322A002.pdf>.
- Soo, P., & Millian, L. (2001). The effect of gamma radiation on the strength of Portland cement mortars. *Journal of materials science letters*, 20(14), 1345–1348.
- Sopko, V., Trtik, K., & Vodák, F. (2004). Influence of  $\gamma$  irradiation on concrete strength. *Acta Polytechnica*, 44(1), 57–58.
- Vodák, F., Trtik, K., Sopko, V., Kapičková, O., & Demo, P. (2005). Effect of  $\gamma$ -irradiation on strength of concrete for nuclear-safety structures. *Cement and Concrete Research*, 35(7), 1447–1451.
- William, K., Xi, Y., & Naus, D. (2013). *A review of the effects of radiation on micro-structure and properties of concretes used in Nuclear Power Plants*: United States Nuclear Regulatory Commission, Office of Nuclear Regulatory Researchs.

## Publisher's Note

Springer Nature remains neutral with regard to jurisdictional claims in published maps and institutional affiliations.

Submit your manuscript to a SpringerOpen® journal and benefit from:

- Convenient online submission
- Rigorous peer review
- Open access: articles freely available online
- High visibility within the field
- Retaining the copyright to your article

Submit your next manuscript at ► [springeropen.com](https://www.springeropen.com)